Hierarchical Columnar RuO2 Nanoplates and Their Improved Cycle Life Performance at High Capacity

ARTICLE *in* THE JOURNAL OF PHYSICAL CHEMISTRY C · JUNE 2014

Impact Factor: 4.77 · DOI: 10.1021/jp5012632

4 AUTHORS, INCLUDING:

Igor Kovalenko
Georgia Institute of Technology
17 PUBLICATIONS **752** CITATIONS

SEE PROFILE

THE JOURNAL OF PHYSICAL CHEMISTRY C

Article

pubs.acs.org/JPCC

Hierarchical Columnar RuO_2 Nanoplates and Their Improved Cycle Life Performance at High Capacity

Anantharamulu Navulla,[†] Geoffrey Stevens,[†] Igor Kovalenko,[‡] and Lamartine Meda*[,†]

[†]Department of Chemistry, Xavier University of Louisiana, 1 Drexel Drive, New Orleans, Louisiana 70125, United States

[‡]School of Materials Science and Engineering, Georgia Institute of Technology, Atlanta, Georgia 30332, United States

ABSTRACT: RuO_2 has been studied for a long time as a model electrode for lithium ion battery, however, little is known about their cycle life at high capacity. Using a simple low-pressure chemical vapor deposition process, hierarchical columnar RuO_2 nanoplates were directly deposited on stainless steel current collectors. Powder X-ray diffraction revealed the existence of the rutile form of RuO_2 ($P42/mnm$, a = 4.499 Å, c = 3.111 Å), with a (110) preferred orientation for the as-deposited materials. The electrodes showed significant cycle life improvement versus Li/Li^+ at high capacity (932 mAh g^{-1}). This capacity is higher than expected for the conversion reaction (806 mAh g^{-1}) of RuO_2. Galvanostatic discharge−charge experiments were performed in the range of 4.0 to 0.1 V versus Li/Li^+ at a constant current density of ∼806 mA g^{-1}. These self-supported electrodes have shown 94% reversibility for the first 30 cycles and 81% after 60 cycles, which indicate good kinetics and excellent capacity retention. This significant improvement in the electrochemical properties is attributed to the growth process and the chemical and mechanical robustness of the electrode.

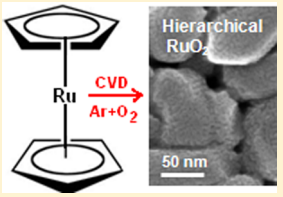

INTRODUCTION

Lithium ion batteries (LIBs) are playing a dominant role in energy storage because of their extensive use in consumer products including cell phones, portable computers, camcorders, I-pods, and medical devices.[1,2] They are now being used in the automotive industry for electric and hybrid vehicles.[3] A typical lithium ion battery is made of two electrodes (anode and cathode) separated by an electrolyte. The most common electrode materials are graphite (372 mAh g^{-1}, anode), $LiCoO_2$ (137 mAh g^{-1}, cathode), and $LiFePO_4$ (170 mAh g^{-1}, cathode).[4] The traditional one electron (insertion/extraction) transfer mechanism into these materials yields low capacity.[5−7] This issue has been addressed by alloying/dealloying and conversion reactions that involved more than one electron. Compounds that were rejected as not having a layered structure, such as RuO_2, CoO, CuO, and NiO, have been shown to react reversibly with lithium.[2,8] Conversion reaction now seems to be common and has been reported for nitrides,[8] sulfides,[9] fluorides,[10] and phosphides.[11] A typical conversion reaction using a divalent metal oxide (M^{+2}) is shown in eq 1.

$$MO + 2Li^+ + 2e^- \leftrightarrow Li_2O + M^0 \quad (1)$$

Conversion reactions are very complex, and their mechanisms are still not very well understood despite intense effort in the past decade.[2,8−11] Now, we are seeing compounds that despite a phase change yield reversible capacity. Among these compounds, RuO_2 is used as a model electrode to elucidate Li reactions with metal oxides.[12,13] It has also been studied extensively as a model electrode for supercapacitor because of its wide potential window for redox reactions, remarkably high specific capacitance, and a very long cycle life.[14−17] Investigations of RuO_2 have been limited to a narrow voltage range and shown moderate reversible capacity.[18−20] Most recently, Balaya et al. demonstrate reversibility in the first cycle between 0.05 and 4.3 V versus Li/Li^+.[21] A high capacity (1130 mAh g^{-1}) that corresponds to the storage of 5.6 Li per mol of RuO_2 and high Coulombic efficiency (98%) is obtained. However, only three cycles are observed before the electrode cracks due to volume expansion that causes the materials to debond from the substrate. Using nanoparticles to improve electrochemical processes is interesting, however extra processing requirements and the need for additives to manufacture a cell may be counterproductive. Direct deposition of the active materials onto current collectors have shown very encouraging electrochemical results for metal oxides.[22]

In this work, using RuO_2 as a model electrode to gain a better understanding of the reactions of Li with metal oxides, we report on the cycle life of hierarchical columnar RuO_2 nanoplates at capacity higher than that expected for RuO_2 conversion reaction. The columnar nanostructures were grown directly on very cheap stainless steel 304L (SS304L) current collectors using a simple low-pressure chemical vapor deposition (LPCVD) process. By using this strategy, the RuO_2 columns are in intimate contact with the current collectors, resulting in improvement in cycle life. Galvanostatic discharge−charge curves of the electrodes show good kinetics and great capacity retention (94% reversibility for 30 cycles and 81% after 60 cycles of their initial capacity, 932 mAh g^{-1}).

EXPERIMENTAL SECTION

RuO_2 Nanoplate Synthesis. Hierarchical columnar RuO_2 nanoplates were deposited on a SS304L (McMaster-Carr)

Received: February 5, 2014
Revised: April 18, 2014
Published: June 2, 2014

   dx.doi.org/10.1021/jp5012632 | J. Phys. Chem. C 2014, 118, 13382−13386

current collector in a LPCVD reactor (Structured Materials, Figure 1). A quartz tube with an inside diameter of approximately 1.5 in. was used, and the SS304L substrates were positioned inside the furnace. All substrates were cleaned prior to use by sonicating in acetone and hexanes and dried with nitrogen. The quartz tube was inserted inside the furnace, and two K-type thermocouples were inserted directly in the tube furnace over the substrates. 50−100 mg (depending on the deposition) of bis(cyclopentadienyl)ruthenium, $Ru(C_5H_5)_2$ (Strem Chemicals), was placed in an alumina boat that was inserted in the quartz tube. Two quick-connect couplings were used to seal both ends of the quartz tube. The reactor chamber was evacuated to a base pressure of 1.6 Pa. The reactor temperature was increased to 400 °C, and then 100 sccm (standard cubic centimeters per minute) of Ar and 100 sccm of O_2 were released to the chamber by slowly opening the shut-off valves. The chamber pressure was set to 4.5 Torr for all the depositions and monitored with an MKS baratron capacitance monometer. A liquid nitrogen trap was placed downstream of the vacuum pump. Swagelok VCR gasket seals were used to maintain a leak free system. The starting precursor was evaporated at 90 °C and transported to the reaction zone for 20 min. Gas flows were stopped, and the furnace was cooled down to room temperature at a rate of 5 °C/min.

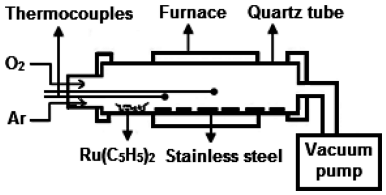

Figure 1. Schematic of the low-pressure chemical vapor deposition (LPCVD) reactor.

Physical Characterization. Powder X-ray powder diffraction (XRD) patterns were collected in a Rigaku diffractometer operating in the conventional Bragg−Brentano geometry and fitted with a monochromator (Cu Kα λ = 1.5405 Å). The morphology and growth architecture were examined in a Hitachi S-4800 field-emission scanning electron microscope (FESEM).

Electrochemical Measurement. The working electrode was 1.24 cm^2 RuO_2 nanoplates on SS304L, and no additives were used. The electrochemical half-cell testing was performed in a Swagelok-type cell using lithium foil as the counter and reference electrode, and Celgard (25 μm thick) as the separator, which was soaked with the electrolyte solution before use. The electrolyte solution was 1.0 M $LiPF_6$ dissolved in a mixture of ethylene carbonate (EC), dimethyl carbonate (DMC), and diethyl carbonate (DEC) with a volume ratio of EC/DMC/DEC of 1:1:1 (MTI). All cells were assembled and tested inside an argon filled glovebox equipped with electrical feed through outposts with H_2O and O_2 pressures <0.5 ppm. Galvanostatic discharge−charge experiments were carried out in a Gamry 600 potentiostat in the voltage window, 4.0−0.1 V up to 60 cycles at a current density of ∼806 mA g^{-1}. Ex situ characterizations were performed by disassembling the cell in the argon glovebox, rinsing with DMC, and drying under vacuum overnight.

RESULTS AND DISCUSSION

Hierarchical columnar RuO_2 nanostructures were directly deposited on SS304L current collectors using LPCVD. This method does not require templates, polymer binder, conductive carbon additives,[23−30] or ex situ metal catalysts.[31] In addition, the materials are chemically bonded to the current collectors, which consequently increases charge transport within the electrode and across the interface due to the shorter diffusion distances and large surface area.

Figure 2 shows representative XRD spectra of the as-deposited RuO_2 nanostructures (Figure 2a) and the amorphous phase after 60 cycles (Figure 2b). The crystal structure of the as-deposited sample was indexed to the standard rutile structure (JCPDS # 21-1172), space group: ($P42/mnm$, a = 4.499 Å, c = 3.111 Å).[32] The additional peaks in the pattern correspond to the SS304L substrates, which are labeled with asterisks. The intensity of the (110) reflection plane is much higher than that of the other reflections in the pattern, which indicates a preferential growth of the (110) plane. No reflections were observed in the XRD pattern of the sample after 60 cycles, which indicates that the material is amorphous.

The as-deposited RuO_2 nanostructures were analyzed by FESEM and are depicted in Figure 3a−c. Plan view images are shown in Figure 3a,b. The surface morphology is quasi-uniform with an average particle diameter of ∼100 nm. A close view high magnification FESEM image (Figure 3b) shows that the nanoplates are ∼5 nm in width and 10 nm in length. A side view image reveals that the nanoplates are self-assembled into columns (Figure 3c). The length of the columns varied in the

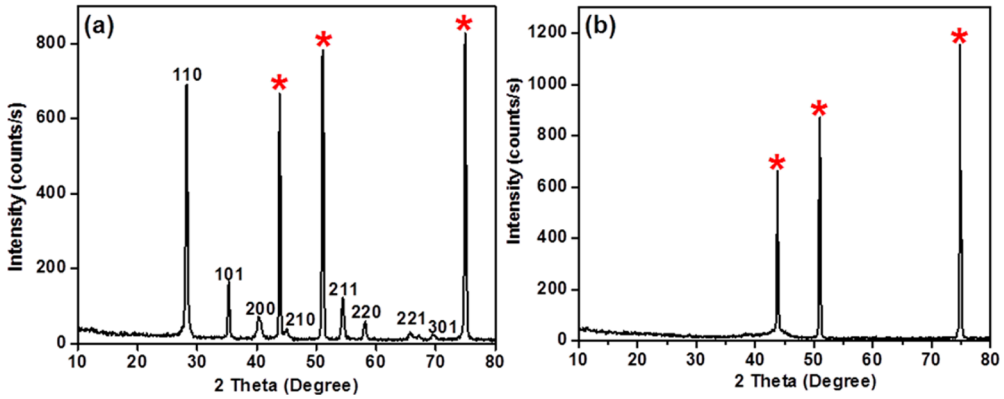

Figure 2. XRD powder patterns (a) of as-deposited hierarchical columnar RuO_2 nanoplates and (b) after 60 discharge−charge cycles. The stainless steel substrate peaks are labeled with asterisks.

dx.doi.org/10.1021/jp5012632 | J. Phys. Chem. C 2014, 118, 13382−13386

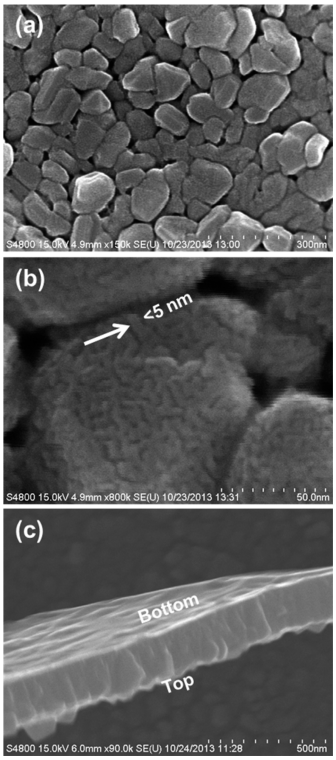

Figure 3. FESEM images of the as-deposited hierarchical columnar RuO_2 nanoplates showing (a) plain view low magnification (150 K) image, (b) plain view high (800 K) magnification image (arrow points to the thickness of a subunit, nanoplate, visible on the surface), and (c) a slab obtained from scratching the surface of a sample.

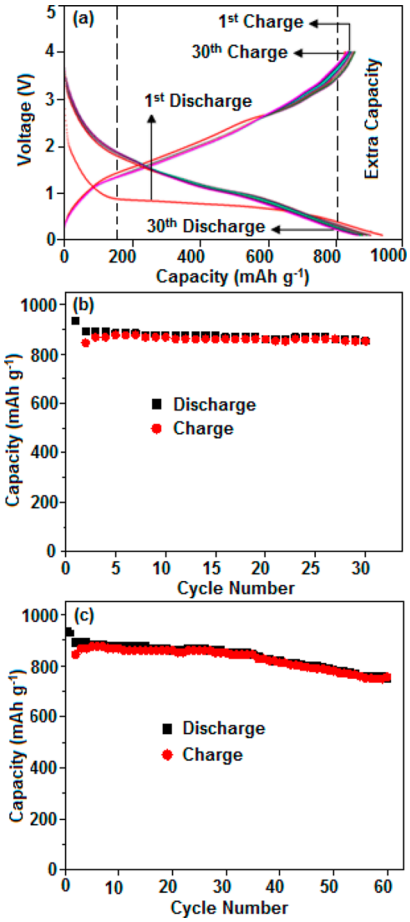

Figure 4. Galvanostatic discharge−charge curves and capacity retention of RuO_2 versus Li/Li^+ in EC/DMC/DEC of 1:1:1 volume ratio at a current density of 806 mAh g^{-1} for a 145 nm thick sample. (a) Voltage versus capacity for the first 30th discharge−charge curves, (b) capacity retention for 30 cycles, and (c) capacity retention for 60 cycles.

range from 145 to 300 nm. Interestingly, it appears that there is an intermediate layer between the RuO_2 columns and the current collector. Indeed, an FESEM picture taken from a slab of a sample confirms the existence of a continuous thin layer of a few nanometers on the bottom of the substrate (Figure 3c). This continuous layer is seen on every deposition independent of the substrates. The composition of the layer is unknown at this time; however, its formation could be responsible for the growth of the RuO_2 nanostructures.

Galvanostatic discharge−charge experiments were performed on 145 nm hierarchical columnar RuO_2 nanoplates. Before each experiment, the current was ramped up quickly from the open-circuit voltage to 4.0 V. Then the cell was continuously cycled between 4.0 and 0.1 V versus Li/Li^+ for up to 60 cycles at a constant current density of 806 mA g^{-1}. We ramped up the current because the open circuit voltage was below the expected lithium intercalation voltage (~2.1 V) of crystalline RuO_2.[21] The mass of the active materials (125.3 μg) was calculated from the thickness and bulk density (6.97 g cm^{-3}) of RuO_2, and the area (1.24 cm^2) of the working electrode.

Figure 4a shows the voltage as a function of capacity for the first 30 cycles. The initial discharge curve shows a sloping region from 4.0 to ~0.8 V that yields 150 mAh g^{-1}(0.74 Li per mol of RuO_2), a plateau at ~0.8 V that provides ~550 mAh g^{-1} (2.73 Li per mol of RuO_2), and a steep slope from 0.8 to 0.1 V which produces an additional ~232 mAh g^{-1} (1.2 Li per mol of RuO_2). The total discharge capacity in the first cycle is ~932 mAh g^{-1} (4.7 Li per mol of RuO_2). This capacity is higher than that expected for RuO_2 by conversion reaction as shown in eq 2:

$$RuO_2 + 4Li \leftrightarrow Ru^0 + 2Li_2O, \quad 806\ \text{mAh g}^{-1} \qquad (2)$$

Based on the initial charge curve, the calculated Coulombic efficiency is >95%, which is significant as far as synthesizing electrode materials for high capacity lithium ion batteries is concerned. Figure 4b shows the capacity as a function of cycle number. It demonstrates that the LPCVD grown RuO_2 nanostructures can be cycled up to 30 times with capacity fading of only ~6% and retained overall 81% of its initial capacity after 60 cycles (Figure 4c). That implies that the electrodes have excellent capacity retention and kinetics. This is indicative of the chemical and mechanical robustness of the electrodes which were able to sustain the structural strains produced by the Li/RuO_2 cell. This was confirmed by FESEM on an electrode after being cycled 60 times, which revealed no peeling or cracking (Figure 5). When compared to published work on Li reactions with RuO_2 nanoparticles,[21] our work demonstrated better electrochemical performance due to better accommodation of the structural strains imposed by the Li/RuO_2 reactions.

In general, during the discharging of Li reactions with crystalline RuO_2, a plateau at ~2.1 V is usually observed that represents the formation of crystalline Li_xRuO_2 ($0 < x < 0.86$) orthorhombic phase.[21] In the present case, we did not observe such a plateau. That could be due to the small crystallite size

dx.doi.org/10.1021/jp5012632 | J. Phys. Chem. C 2014, 118, 13382−13386

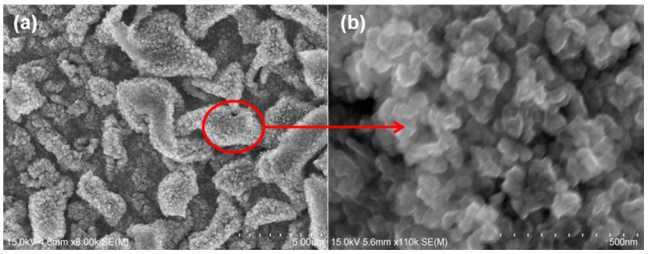

Figure 5. FESEM images taken from a fully discharged Li/RuO_2 cell after 60 cycles. Plan view photographs obtained at different resolutions are shown in panels a and b.

(<5 nm) of the RuO_2 nanostructure which plays an important role in determining the initial discharge profile characteristics.[33] The discharge plateau at approximately 0.8 V represents the formation of the solid electrolyte interface (SEI) layer and the conversion reaction (reduction) of Ru ions to Ru metal nanosize and amorphous Li_2O. The reduction reaction has been confirmed by Balaya et al., who have observed the Ru and Li_2O mixed phase by selected area electron diffraction (SAED) using RuO_2 nanoparticles.[21] Their results have been confirmed by Bekaert et al. using solid-state NMR.[34] Therefore, we concluded that the hierarchical columnar RuO_2 underwent a conversion reaction at deep discharge voltages similar to the aforementioned RuO_2 nanoparticles. Indeed, a typical conversion reaction trend is seen in the second discharge curve with no indication of a plateau. This is due to the amorphization of RuO_2 upon charging, where the decomposition of the Li_2O amorphous phase is kinetically enhanced by the Ru metal nanosize (Figure 2b). It is worth mentioning that an overall increase in the average voltage in the second discharge curve was observed. This increase in voltage, which leads to a hysteresis, is very common in conversion reaction of 3d metal oxides.[22]

We have collected physical evidence by ex situ XRD and FESEM on a fully discharged sample after 60 cycles. These results provide physical insight regarding the structural evolution of the electrode. The XRD spectrum in Figure 2b shows that the material is amorphous because no reflections characteristics of a long-range order were observed besides those of the substrate. Figure 5 shows FESEM images of the sample and the transformation from columnar nanoarchitecture (as-deposited) to nanoparticles. Figure 5a shows a low magnification image, which reveals no cracking or mechanical defect in the electrode. Closer plan view FESEM images (Figure 5b) show the rearrangement of the morphology of the electrode surface into nanodomains of ∼50 nm. Clearly, the interconnectivity of the nanodomains (Ru/Li_2O) is maintained, which points to effective transport within the material and across the interface, therefore improving the cell kinetics. However, the distribution of the Ru metal in the Li_2O mixed phase in the nanodomains is not clear at this time, but a network of Ru−Ru metal may provide the pathway that allows the transport of electrons to and from the electrode. Understanding of charge transport in these nanodomains is a challenging issue due to their in situ formation and the range of disorder that they exhibit.

Between the first and the second discharge curves, the electrode shows 97% reversibility. The Coulombic efficiency was ∼95% between the first discharge−charge cycles and rose to almost 100% and remained stable during subsequent cycling (Figure 4a). This shows that Li losses due to the formation of the SEI layer are not significant during the first 30 cycles as it relates to the reversibility of RuO_2. It is known, however, that SEI formation takes place and decomposes in the investigated voltage range.[21] In our case, the SEI formation is not detrimental to the material because capacity loss during the first few cycles was almost negligible. Interestingly, the extra capacity was retained (for at least 30 cycles, Figure 4a) despite the SEI formation. The origin of the extra capacity is not clearly understood at this time. However, published results have shown that interfacial storage is the dominant mechanism for the extra capacity.[21] In the RuO_2 nanoparticle study by Balaya et al., the extra capacity is the steep slope that starts exactly at 4 Li per mol of RuO_2 (∼0.8 V), while in our case the steep slope starts at ∼1 V and is seen on every discharge cycle. This slope is the transition to complete formation of Ru and Li_2O as shown in the NMR study.[34] Also, there is a possibility that reactions of Li with the electrolyte, which was demonstrated in the CoO/Li cell to form a pseudocapacitive polymer/gel like film material, could add to the extra capacity.[35] Recently, Clare P. Gray et al. proposed that generation of LiOH and its subsequent reversible combination with extra Li to form Li_2O and LiH is responsible for the extra capacity.[36] Therefore, it is difficult to say which mechanism is responsible for the observed capacity at low voltages.[21,35,36]

■ CONCLUSIONS

In conclusion, a simple LPCVD process was used to synthesize hierarchical columnar RuO_2 directly on stainless steel current collector. As-prepared electrodes were crystalline according to powder XRD, and FESEM revealed columnar nanoarchitecture made of 5 nm building blocks. The materials became amorphous after 60 cycles. This is very common for materials that undergo conversion reactions. Galvanostatic discharge−charge experiments demonstrated exceptional capacity retention of 94% after 30 cycles and 81% after 60 cycles. These self-supported electrodes show better rate capabilities (good kinetics) than RuO_2 nanoparticle electrodes. Our electrodes were able to accommodate the structural strains imposed by the Li/RuO_2 reactions that favor a longer cycle life due to the LPCVD growth process and the chemical and mechanical robustness of the electrode. This was confirmed by FESEM photographs taken after 60 cycles, which reveal no peeling or cracking of the electrodes. The high cost of the material, significant voltage hysteresis, and smaller capacitance in a more narrow potential range will likely prevent its commercial use. However, as a model electrode, significant insights were obtained regarding Li reactions with metal oxides in conversion reaction. These results can be extrapolated to other materials such as iron oxide and manganese oxide anode materials which are more suitable for battery application.

■ AUTHOR INFORMATION

Corresponding Author

*Phone: 1-504-520-5324. Fax: 1-504-520-7942. E-mail: LMeda@Xula.edu.

Notes

The authors declare no competing financial interest.

■ ACKNOWLEDGMENTS

The authors would like to thank the National Science Foundation through the Partnership for Research and Education in Materials program (NSF-PREM) Award Number

DMR-0934111 for their financial support. We also want to acknowledge the NSF EPSCoR Cooperative Agreement No. EPS-1003897 with additional support from the Louisiana Board of Regents for their financial support of G.S. We want to thank Richard Graves for his assistance with the FESEM images. The authors are grateful for Dr. Feffrey Fergus from Auburn University and Dr. Gleb Yushin from Georgia Institute of Technology for reviewing the manuscript and useful discussions.

REFERENCES

(1) Tarascon, J.-M.; Armand, M. Issues and Challenges Facing Rechargeable Lithium Batteries. *Nature* **2001**, *414*, 359−367.
(2) Bruce, Peter G.; Scrosati, B.; Tarascon, J.-M. Nanomaterials for Rechargeable Lithium Batteries. *Angew. Chem., Int. Ed.* **2008**, *47*, 2930−2946.
(3) Tarascon, J.-M.; Recham, N.; Armand, M.; Chotard, J.-N.; Barpanda, P.; Walker, W.; Dupont, L. Hunting for Better Li-Based Electrode Materials *via* Low Temperature Inorganic Synthesis. *Chem. Mater.* **2010**, *22*, 724−739.
(4) Angara, T.; Tozawa, K. Lithium Ion Rechargeable Battery. *Prog. Batteries Sol. Cells* **1990**, *9*, 209−217.
(5) Li, H.; Wang, Z.; Chen, L.; Huang, X. Research on Advanced Materials for Li-ion Batteries. *Adv. Mater.* **2009**, *21*, 4593−4607.
(6) Manthiram, A. Materials Challenges and Opportunities of Lithium Ion Batteries. *J. Phys. Chem. Lett.* **2011**, *2*, 176−184.
(7) Praveen, M.; Chandrashekhar, P.; Kumar, V.; Sumanasekera, G. U.; Sunkara, M. K. Hybrid Tin Oxide Nanowires as Stable and High Capacity Anodes for Li-Ion Batteries. *Nano Lett.* **2009**, *9*, 612−616.
(8) Pereira, N.; Dupont, L.; Tarascon, J.-M.; Klein, L. C.; Amatucci, G. G. Electrochemistry of Cu_3N with Lithium: A Complex System with Parallel Process. *J. Electrochem. Soc.* **2003**, *150*, A1273−A1280.
(9) Poizot, P.; Laruelle, S.; Grugeon, S.; Dupont, L.; Beaudoin, B.; Tarascon, J.-M. Réactivité et réversibilité électrochimiques d'oxydes de cobalt vis-à-vis du lithium. *C. R. Acad. Sci., Ser. IIc: Chim.* **2000**, *3*, 681−691.
(10) Li, H.; Richter, G.; Maier, J. Reversible Formation and Decomposition of LiF Clusters Using Transition Metal Fluorides as Precursors and Their Application in Rechargeable Li Batteries. *Adv. Mater.* **2003**, *15*, 736−739.
(11) Pralong, V.; Souza, D. C. S.; Leung, K. T.; Nazar, L. Reversible Lithium Uptake by CoP_3 at Low Potential: Role of the Anion. *Electrochem. Commun.* **2002**, *4*, 516−520.
(12) Wang, X.; Gordon, R. G. High-Quality Epitaxy of Ruthenium Dioxide, RuO_2, on Rutile Titanium Dioxide, TiO_2, by Pulsed Chemical Vapor Deposition. *Cryst. Growth Des.* **2013**, *13*, 1316−1321.
(13) Gujar, T. P.; Kim, W.-Y.; Puspitasari, I.; Jung, K. D.; Joo, O.-S. Electrochemically Deposited Nanograin Ruthenium Oxide as a Pseudocapacitive Electrode. *Int. J. Electrochem. Sci.* **2007**, *2*, 666−673.
(14) Patake, V. D.; Lokhande, C. D.; Joo, O.-S. Electrodeposited Ruthenium Oxide Thin Films for Supercapacitor: Effect of Surface Treatments. *Appl. Surf. Sci.* **2009**, *255*, 4192−4196.
(15) Jirkoversusky, J.; Makarova, M.; Krtil, P. The Effect of Coherent Domain Size on the Insertion Activity of Nanocrystalline RuO_2. *J. Electrochem. Soc.* **2005**, *152*, A1613−A1619.
(16) Lytle, J. C.; Rhodes, C. P.; Long, J. W.; Pettigrew, K. A.; Stroud, R. M.; Rolison, D. R. The Importance of Combining Disorder with Order for Li-ion Insertion into Cryogenically Prepared Nanoscopic Ruthenia. *J. Mater. Chem.* **2007**, *17*, 1292−1299.
(17) Kuratani, K.; Kiyobayashi, T.; Kuriyama, N. Influence of the Mesoporous Structure on Capacitance of the RuO_2 Electrode. *J. Power Sources* **2009**, *189*, 1284−1291.
(18) Murphy, D. W.; Di Salvo, F. J.; Carides, J. N.; Waszczak, J. V. Topochemical Reactions of Rutile Related Structures with Lithium. *Mater. Res. Bull.* **1978**, *13*, 1395−1402.
(19) Dalard, P.; Deroo, D.; Foscallo, D.; Mouliom, C. A Galvanostatic Study of Lithium Intercalation in RuO_2. *Solid State Ionics* **1985**, *15*, 91−94.
(20) Armand, M.; Dalard, F.; Deroo, D.; Mouliom, C. Modelling the Voltammetric Study of Intercalation in a Host Structure: Application to Lithium Intercalation in RuO_2. *Solid State Ionics* **1985**, *15*, 205−210.
(21) Balaya, P.; Li, H.; Kienle, L.; Maier, J. Fully Reversible Homogeneous and Heterogeneous Li Storage in RuO_2 with High Capacity. *Adv. Funct. Mater.* **2003**, *13*, 621−625.
(22) Tabernal, P. L.; Mitra, S.; Poizot, P.; Simon, P.; Tarascon, J.-M. High Rate Capabilities Fe_3O_4-Based Cu Nano-architectured Electrodes for Lithium-ion Battery Applications. *Nat. Mater.* **2006**, *5*, 567−573.
(23) Sim, D. H.; Rui, X.; Chen, J.; Tan, H.; Lim, T. M.; Yazami, R.; Hng, H. H.; Yan, Q. Direct Growth of $FeVO_4$ Nanosheet Arrays on Stainless Steel Foil as High-Performance Binder-Free Li Ion Battery Anode. *RSC Adv.* **2012**, *2*, 3630−3633.
(24) Song, Y. Q.; Qin, S. S.; Zhang, Y. W.; Gao, W. Q.; Liu, J. P. Large-Scale Porous Hematite Nanorod Arrays: Direct Growth on Titanium Foil and Reversible Lithium Storage. *J. Phys. Chem. C* **2010**, *114*, 21158−21164.
(25) Liu, J. P.; Li, Y. Y.; Huang, X. T.; Ding, R. M.; Hu, Y. Y.; Jiang, J.; Liao, L. Direct Growth of SnO_2 Nanorod Array Electrodes for Lithium-Ion Batteries. *J. Mater. Chem.* **2009**, *19*, 1859−1864.
(26) Fan, Y. Q.; Shao, H. B.; Wang, J. M.; Liu, L. A.; Zhang, J. Q.; Cao, C. N. Synthesis of Foam-Like Freestanding Co_3O_4 Nanosheets with Enhanced Electrochemical Activities. *Chem. Commun.* **2011**, *47*, 3469−3471.
(27) Li, Y. G.; Tan, B.; Wu, Y. Y. Mesoporous Co_3O_4 Nanowire Arrays for Lithium Ion Batteries with High Capacity and Rate Capability. *Nano Lett.* **2008**, *8*, 265−270.
(28) Saadat, S.; Tay, Y. Y.; Zhu, J. X.; Teh, P. F.; Maleksaeedi, S.; Shahjamali, M. M.; Shakerzadeh, M.; Srinivasan, M.; Tay, B. Y.; Hng, H. H.; et al. Template-Free Electrochemical Deposition of Interconnected ZnSb Nanoflakes for Li-Ion Battery Anodes. *Chem. Mater.* **2011**, *23*, 1032−1038.
(29) Liu, R.; Duay, J.; Lee, S. B. Heterogeneous Nanostructured Electrode Materials for Electrochemical Energy Storage. *Chem. Commun.* **2011**, *47*, 1384−1404.
(30) Chan, C. K.; Peng, H. L.; Liu, G.; McIlwrath, K.; Zhang, X. F.; Huggins, R. A.; Cui, Y. High-Performance Lithium Battery Anodes Using Silicon Nanowires. *Nat. Nanotechnol.* **2008**, *3*, 31−35.
(31) Seo, J.-w.; Jang, J.-t.; Park, S.-w.; Kim, C.; Park, B.; Cheon, J. Two-Dimensional SnS_2 Nanoplates with Extraordinary High Discharge Capacity for Lithium Ion Batteries. *Adv. Mater.* **2008**, *20*, 4269−4273.
(32) Bolzan, A. A.; Fong, C.; Kennedy, B. J.; Howard, C. J. Structural Studies of Rutile-Type Metal Dioxides. *Acta Crystallogr., Sect. B: Struct. Sci.* **1997**, *53*, 373−380.
(33) Guo, J.; Liu, Q.; Wang, C.; Zachariah, R. M. Interdispersed Amrophous MnOx-Carbon Nanocomposites with Superior Electrochemical Performance as Lithium-Storage Material. *Adv. Funct. Mater.* **2012**, *22*, 803−811.
(34) Bekaert, E.; Balaya, P.; Murugavel, S.; Maier, J.; Ménétrier, M. Li MAS NMR Investigation of Electrochemical Lithiation of RuO_2: Evidence for an Interfacial Storage Mechanism. *Chem. Mater.* **2009**, *21*, 856−861.
(35) Laruelle, S.; Grugeon, S.; Poizot, P.; Dolle, M.; Dupont, L.; Tarascon, J.-M. On the Origin of the Extra Electrochemical Capacity Displayed by MO/Li Cells at Low Potential. *J. Electrochem. Soc.* **2002**, *149*, A627−A634.
(36) Hu, Y.-Y; Liu, Z.; Nam, K.-W.; Borkiewicz, O. J.; Cheng, J.; Hua, X.; Dunstan, M. T.; Yu, X.; Wiaderek, K. M.; Du, L.-S.; et al. Origin of Additional Capacities in Metal Oxide Lithium-ion Battery Electrodes. *Nat. Mater.* **2013**, *12*, 1130−1136.